Biophysical Journal, Volume *118*

Supplemental Information

Electrostatic Environment of Proteorhodopsin Affects the pKa of Its Buried Primary Proton Acceptor

Chung-Ta Han, Jichao Song, Tristan Chan, Christine Pruett, and Songi Han

SUPPORTING MATERIALS

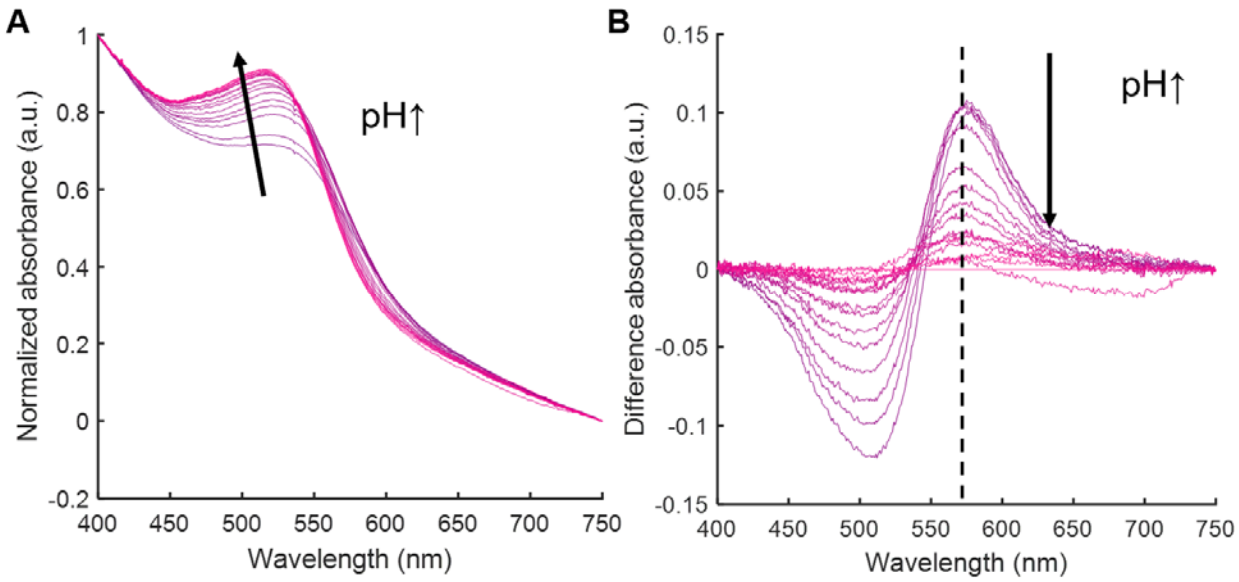

FIGURE S1 pH-dependence optical absorbance change was used to map out the pKa_{D97} of PR. A. The background subtracted optical absorbance of PR under a range between 400 and 750 nm, which showed a pH-dependent absorbance change. B. The difference absorbance of PR between 400 and 750 nm under various pH in the spectral titration experiments. The difference absorbance is calculated by subtracting each spectrum with the one measured under the most basic condition in that set of spectral titration experiment. The value of difference absorbance at 570 nm (indicated by the dotted line) was normalized and plotted against the measured bulk pH to get the titration curve as shown in Figure 1.

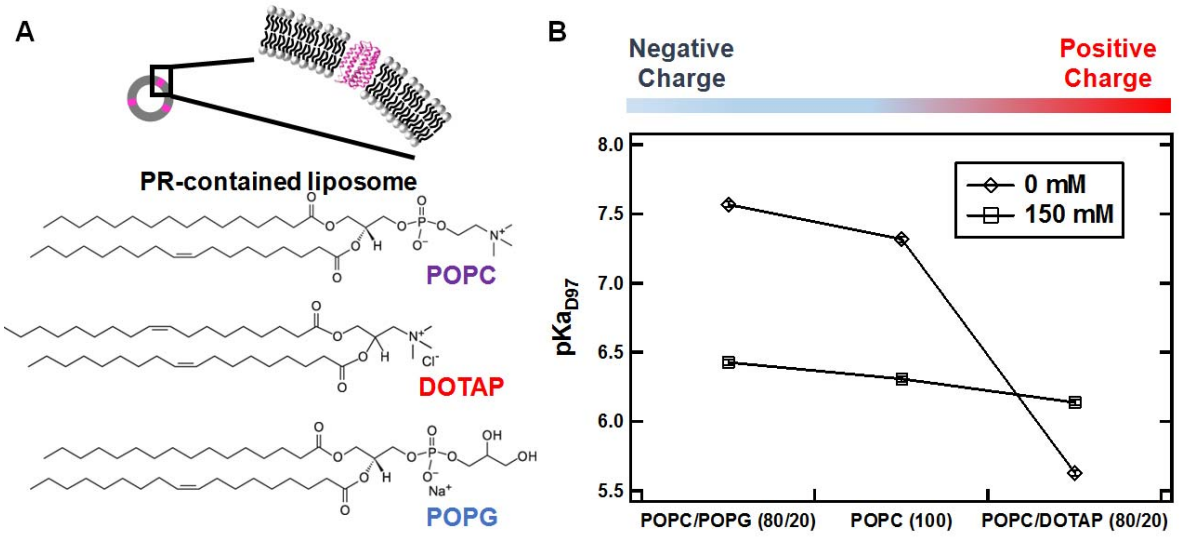

FIGURE S2 A. A Schematic diagram of PR-contained liposomes and chemical structures of the lipids used in this study: zwitterionic POPC, positively-charged DOTAP, and negatively-charged POPG. B. Apparent pKa_{D97} of WT PR reconstituted in negatively-charged POPC/POPG (80/20, mol/mol), pure zwitterionic POPC, and positively-charged POPC/DOTAP (80/20, mol/mol) liposomes in a HEPES buffer without additional NaCl (diamond) and the buffer with additional 150 mM NaCl (square).

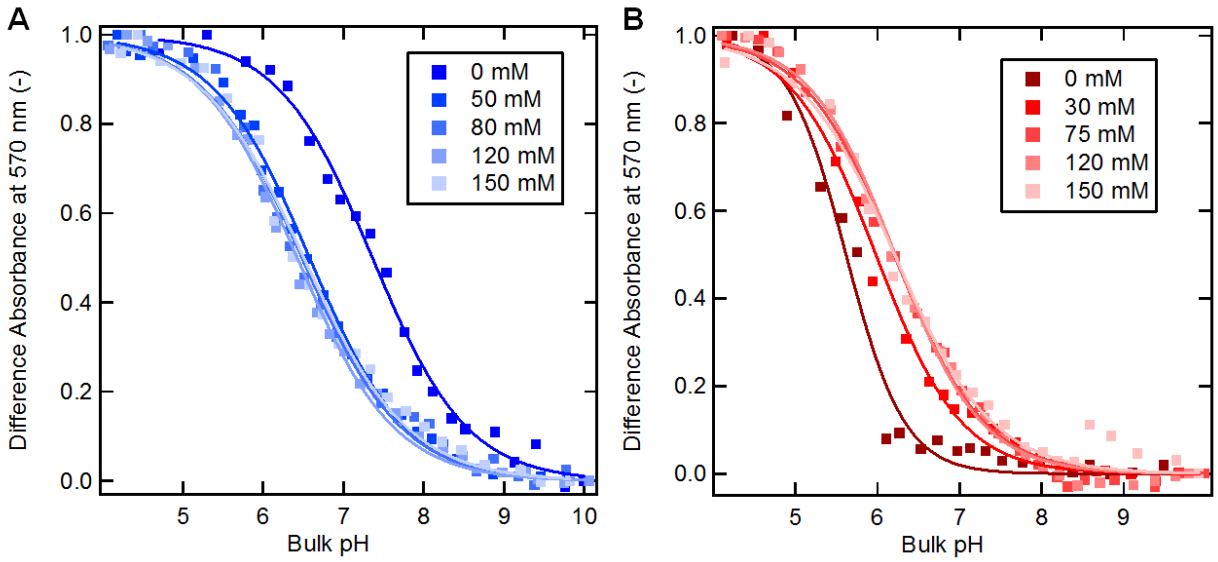

FIGURE S3 Difference optical absorbance at 570 nm under various bulk pH from WT PR reconstituted in A. negatively-charged POPC/POPG (80/20, mol/mol) liposomes and B. positively-charged POPC/DOTAP (80/20, mol/mol) liposomes in HEPES buffer contained different concentrations of NaCl.

Using Gouy-Chapman theory to calculate the surface pH for spectral titration experiments

Proton concentration on a charged liposome surface can differ from its concentration in the bulk solution. This concentration difference highly depends on the electrostatic potential on the charged liposome surface. Briefly, proton can be absorbed on a negatively-charged surface based on the double-layer theory, and results in a lower surface proton concentration in comparison to the bulk concentration. In contrary, a positively-charged liposome surface can repel protons and results in a higher surface proton concentration in comparison to the bulk concentration. The relationship between the proton concentration difference and the surface potential ψ_0 can be described by the Nernst equation

$$pH_{surface} = pH_{bulk} + \frac{zF\psi_0}{2.303RT}, \quad (1)$$

where z is the ion charge, which is +1 for proton, F is the Faraday constant, R is the ideal gas constant and T is the absolute temperature. The surface potential ψ_0 is related to the surface charge density σ. With an assumption that the liposome surface is a static and flat surface, we can use the Gouy-Chapman model to correlate the surface potential ψ_0 with the membrane surface charge density σ

$$\sigma = \sqrt{8000kT\varepsilon_0\varepsilon C_{el}N_A} \cdot \sinh\left(\frac{zF\psi_0}{2RT}\right), \quad (2)$$

where k is the Boltzmann constant, ε_0 is the vacuum permeability constant, N_A is the Avogadro constant, ε is the dielectric constant, for water $\varepsilon = 78$, and C_{el} is the electrolyte concentration, which is the concentration of applied salt with monovalent or divalent cations in the buffer. In order to resolve the surface potential ψ_0, we have to calculate the surface charge density σ. The surface charge density of a charged species i can be expressed as

$$\sigma_i = \frac{ze\alpha}{A_{L,i}}, \quad (3)$$

where e is the elementary charge, $A_{L,i}$ is the surface area per ionizable group of a lipid (0.597 nm^2 for PC (1), 0.61 nm^2 for DOTAP (2), 0.65 nm^2 for POPG (3)), and α is the degree of dissociation of an ionizable group that determines the percentage of it in its charged form. For example, in the case of POPC, it contains a phosphorous group that can distribute between a negatively charged form and a neutral form while it is associated with protons or other cations (e.g. Na). The degree of dissociation of this phosphorous group can be expressed as

$$\alpha_{PC,PO_4^-} = \frac{1}{1+\left(\frac{[H_3O^+]}{K_H}+\frac{[Na^+]}{K_{Na}}\right)exp\left(-\frac{F\psi_0}{RT}\right)} \quad (4)$$

where $[H_3O^+]$ and $[Na^+]$ are the proton and sodium concentration in the buffer, respectively. K_H and K_{Na} are the dissociation constant for the binding of proton and sodium to the phosphorous group, respectively. All the parameters for calculating the surface charge density of different ionizable headgroups are obtained from literature (4). The surface charge density σ of all the ionizable groups, including the aforementioned phosphorous group on lipids, can then be combined based on the ratio between different lipid species using the following equation:

$$\sigma = \sum_i x_i \sigma_i \quad (5)$$

By solving the nonlinear equations between (2) and (5), the surface potential ψ_0 on the charged liposome surface can be obtained. The surface potential ψ_0 under different bulk pH then can be used to calculate surface proton concentrations in a spectral titration experiment. The converted surface proton concentration series for each spectral titration experiment then was fitted by the Henderson-Hasselbalch equation to get the intrinsic pKa_{D97}. This value represents the intrinsic acid dissociation constant of the D97 residue, while the apparent pKa does not take the surface proton concentration difference into account. The intrinsic pKa_{D97} still clearly changes for PR reconstituted in liposomes with different net charges and in buffers with different NaCl concentrations (Table S1).

TABLE S1 Intrinsic pKa_{D97} and corresponding apparent pKaD97 of PR reconstituted in liposomes with different net charges and in buffers with different NaCl concentrations. The surface potential on liposomes is predicted by the Gouy-Chapman model.

POPC/POPG (80/20)				POPC/DOTAP (80/20)			
NaCl (mM)	$pKa_{D97,\ intrinsic}$	$pKa_{D97,\ apparent}$	ψ_0 (mV)	NaCl (mM)	$pKa_{D97,\ intrinsic}$	$pKa_{D97,\ apparent}$	ψ_0 (mV)
0	5.11	7.62	-142	0	7.64	5.63	116
50	5.53	6.79	-72	30	6.74	5.90	48
80	5.54	6.62	-62	75	6.65	6.14	29
120	5.60	6.51	-53	120	6.52	6.14	22
150	5.74	6.43	-40	150	6.42	6.14	16

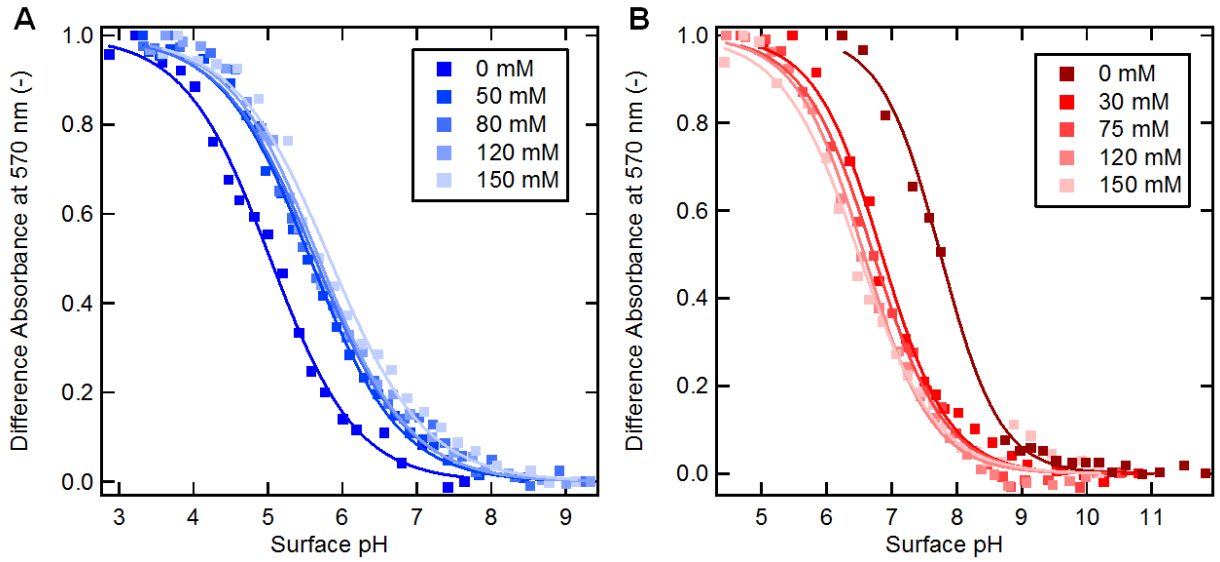

FIGURE S4 Difference optical absorbance at 570 nm plotted against surface pH predicted by the Gouy-Chapman model from WT PR reconstituted in A. negatively-charged POPC/POPG (80/20, mol/mol) liposomes and B. positively-charged POPC/DOTAP (80/20, mol/mol) liposomes in HEPES buffer contained different concentrations of NaCl.

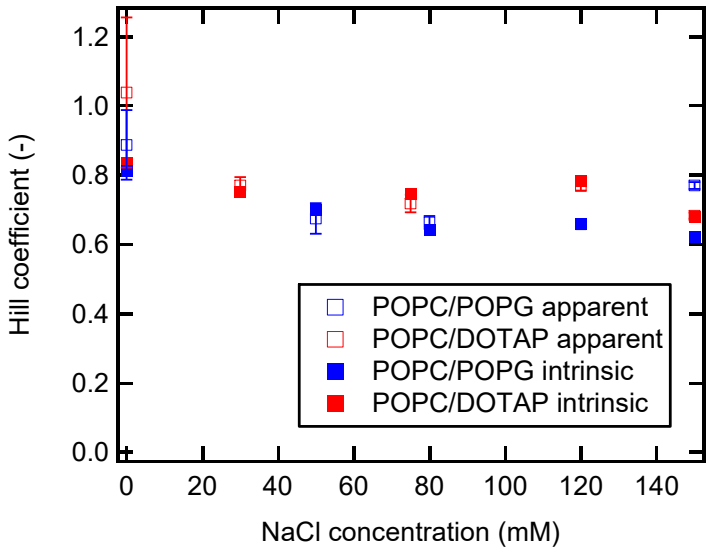

FIGURE S5 Hill coefficients from the Henderson-Hasselbalch fitting for both the apparent pKa_{D97} (hollow squares) and the intrinsic pKa_{D97} (filled squares) of WT PR reconstituted in negatively-charged POPC/POPG (80/20, mol/mol) liposomes (blue) and positively-charged (80/20, mol/mol) liposomes (red) in a 10 mM HEPES buffer. The HEPES buffer contained different concentrations of NaCl between 0 mM and 150 mM.

Overhauser DNP analysis for obtaining hydration dynamics

The details of Overhauser DNP theory, hardware setup, and data analysis for hydration dynamic measurements were described in literatures (5-7). Here, basic principles of ODNP are included for explaining how hydration dynamics on the E-F loop of proteorhodopsin (PR) in this study were obtained. ODNP relaxometries can distinctively measure the hydration dynamics within 5-10 Å from a spin-labeled biological surface with nitroxide radicals. This information is extracted from the change of water ^{1}H NMR signal enhancements under various microwave irradiation powers. Once a microwave irradiation is applied to the samples with spin-labeled biological surfaces, electron spins with higher polarization will transfer the energy through cross-relaxation to the ^{1}H nuclei on water molecules to achieve ^{1}H NMR signal enhancements, and this effect is dominated by the time-dependent dipolar coupling between the electron and proton spins. Since the dipolar coupling is short-range and distance-dependent, the NMR enhancement is solely limited to water molecules within 5-10 Å from the electron spins on spin labels. With these characteristics, this technique becomes a unique and powerful method to study local water dynamics on the surface of biomolecules that could provide underlying structural and functional information (8-11).

The relationship between NMR signal enhancements and fitting parameters with water dynamic information can be derived from the equation of motion for polarization of proton spins interacting with electron spins on nitroxide radicals as below:

$$\frac{d\langle I_z\rangle}{dt} = -(\omega_0 + 2\omega_1 + \omega_2 + \omega^0)(\langle I_z\rangle - I_0) - (\omega_2 - \omega_0)(\langle S_z\rangle - S_0) \quad (6)$$

where $\langle I_z\rangle$ and $\langle S_z\rangle$ are nuclear and electron magnetizations under microwave irradiations, respectively. I_0 and S_0 are nuclear and electron spin equilibrium magnetizations without microwave irradiation, respectively. ω_0, ω_1, and ω_2 are zero-, single-, and double-quantum transition rates, which all represent transition probabilities of spin populations between different energy states. The first term here can be separated into two parts, where $\omega_0 + 2\omega_1 + \omega_2$ can be defined as self-relaxation rate ρ and ω^0 is the nuclear spin relaxation ($T_{1,0}{}^{-1}$) unrelated to paramagnetic relaxation. The second term $\omega_2 - \omega_0$ can be defined as cross-relaxation rate σ. After substituting in these definitions, the steady-state solution of Eq. 1 under continuous microwave irradiation leads an expression of NMR signal enhancement E, which is the ratio between $\langle I_z\rangle$ and I_0.

$$E = 1 - \frac{\sigma}{\rho + T_{1,0}{}^{-1}} \cdot \frac{S_0 - \langle S_z\rangle}{S_0} \cdot \frac{|\gamma_S|}{\gamma_I} \quad (7)$$

where $|\gamma_S|/\gamma_I$ is the ratio of electron and proton gyromagnetic ratios, which is close to 660. The cross-relaxation rate σ can be expressed as a product of spin label concentration C_{SL} and cross-relaxivity k_σ, which is exclusively sensitive to changes in the fast water diffusivity with correlation times of order few to hundreds of ps. A few terms in Eq. 2 can be further simplified and defined as below:

$$s(p) = \frac{S_0 - \langle S_z\rangle}{S_0} \quad (8)$$

$$T_1(p)^{-1} = \rho + T_{1,0}{}^{-1} \quad (9)$$

where s is the saturation factor as a function of microwave irradiation power p, which would asymptotically approach a maximum value s_{max} with an increment of the microwave power. For most of the biological samples with tethered spin labels that have slow tumbling rate, an approximation of $s_{max} \approx 1$ is valid(5, 6). T_1 is the spin lattice relaxation rate of the system with spin labels, which is also a function of microwave power p. By applying Eq. 3 and Eq. 4, Equation 2 can be further reorganized as below:

$$k_\sigma = \frac{1}{C_{SL}} \frac{\gamma_I}{|\gamma_S|} \lim_{p\to\infty} \left(\frac{1-\mathrm{E}(p)}{T_1(p)s(p)} \right) \tag{10}$$

In order to obtain the cross-relaxivity k_σ, the terms that are functions of microwave irradiation power p are extrapolated to infinite power, as the saturation factor s is known to be 1 under this condition. The NMR signal enhancement E and the spin lattice relaxation rate T_1 can be experimentally measured through separate measurements under various microwave irradiation powers. The ^{1}H enhancement series were done by single pulse experiments and the T_1 was measured through inversion recovery measurements. The combination of E and T_1 under different microwave irradiation powers with other constants and spin label concentration C_{CL} are plotted as shown in Figure S4, and the trend is extrapolated to an infinite power for getting the reported k_σ in the main text for different conditions.

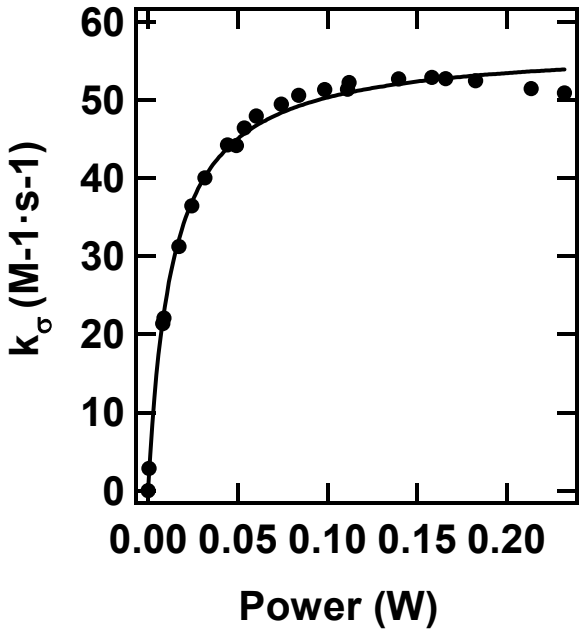

Figure S6 ^{1}H Overhauser dynamic nuclear polarization (ODNP) enhancement series of PR reconstituted in negatively-charged POPC/POPG (80/20, mol/mol) liposomes as an example of how the fitting in Equation 5 is done to obtain the cross-relaxivity k_σ.

Measure the hydration dynamics at the lipid-water interface using MTSL-labeled C-WALP23

MTSL-labeled C-WALP23 peptide is used as a control to measure the hydration dynamics at the lipid-water interface, which is the location of the E-F loop on PR in lipid bilayers. This control can help us to verify whether the observed hydration dynamics change on the site 174 on the E-F loop of PR in Fig. 4 is uniquely caused by a change of its structure or solely a change of lipid environment experienced by the transmembrane protein (TMP). WALP peptide is commonly used as a model of TMP embedded in a lipid bilayer (12-14). The name of this peptide is an abbreviation of alternating hydrophobic alanine (A) and leucine (L) that forms an α-helical transmembrane structure and four membrane-anchoring tryptophans (W) at the membrane-water interface. The C-WALP23 peptide used here has an amino acid sequence provided in Fig. S3(a), with an additional cysteine (C) added above the tryptophans to mimic the location of the E-F loop on PR reconstituted in lipid bilayers. The cysteine residue is conjugated with a MTSL spin label for measuring the hydration dynamics around the membrane-water interface using ODNP. For MTSL-labeled C-WALP23 reconstituted in negatively-charged POPC/POPG (80/20, mol/mol) liposomes, 150 mM in the HEPES buffer led to a higher cross-relaxivity k_σ ($28.3 \pm 2.5\ s^{-1}$) compared to with 0 mM NaCl ($k_\sigma = 26.4 \pm 1.6\ s^{-1}$), in contrast to a drop of k_σ from $52.6 \pm 4.5\ s^{-1}$ to $44.2 \pm 2.5\ s^{-1}$ with the presence of 150 mM measured from site 174 on the E-F loop of PR The opposite trend of hydration changes in these two cases prove that the observed decrement of k_σ on site 174 is caused by the change of local structure around 174, but not solely the change of lipid hydration experienced by the reconstituted TMP.

The C-WALP23 peptide was synthesized by RS Synthesis (Louisville, KY). We mainly followed the protocol published by Lueders et al. to prepare MTSL spin labeled WALP23 peptides(15). The spin labeled WALP peptides dissolved in trifluoroethanol (TFE) was added to lipids with a 1:2200 peptide-to-lipid molar ratio. The lipid vesicles with WALP peptides were prepared by the extrusion method described in the Method section to form lipid vesicles with 200 nm in diameter. All the WALP-contained liposomes were equilibrated in the same HEPES buffer as used for PR samples with the desired NaCl concentration.

A

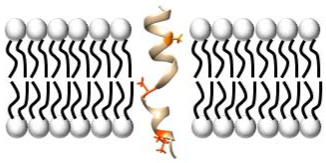

C-WALP23
peptide

Name	Peptide Sequence	MW
C-WALP23	Ac-C(sl)GWWLALA LALALALALALAL WWA-NH_2	2643.512

B

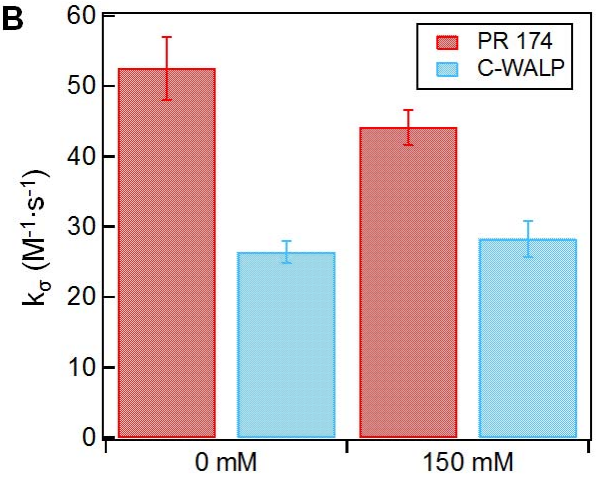

FIGURE S7 A. The cysteine residue conjugated with MTSL spin labels located on the top of the α-helix structure of WALP23 peptides mimic the location of E-F loop on PR reconstituted in lipid bilayers. The peptide sequence and its molecule weight of the C-WALP23 are included in the inlet table. B. The comparison of cross-relaxivities k_σ measured by ODNP between MTSL-labeled C-WALP in POPC/POPG (80/20, mol/mol) and PR with MTSL spin label on site 174 (values reported in Figure 4) in a HEPES buffer with and without 150 mM NaCl. The liposomes samples with the C-WALP23 peptide or PR are all equilibrated at pH 8.5.

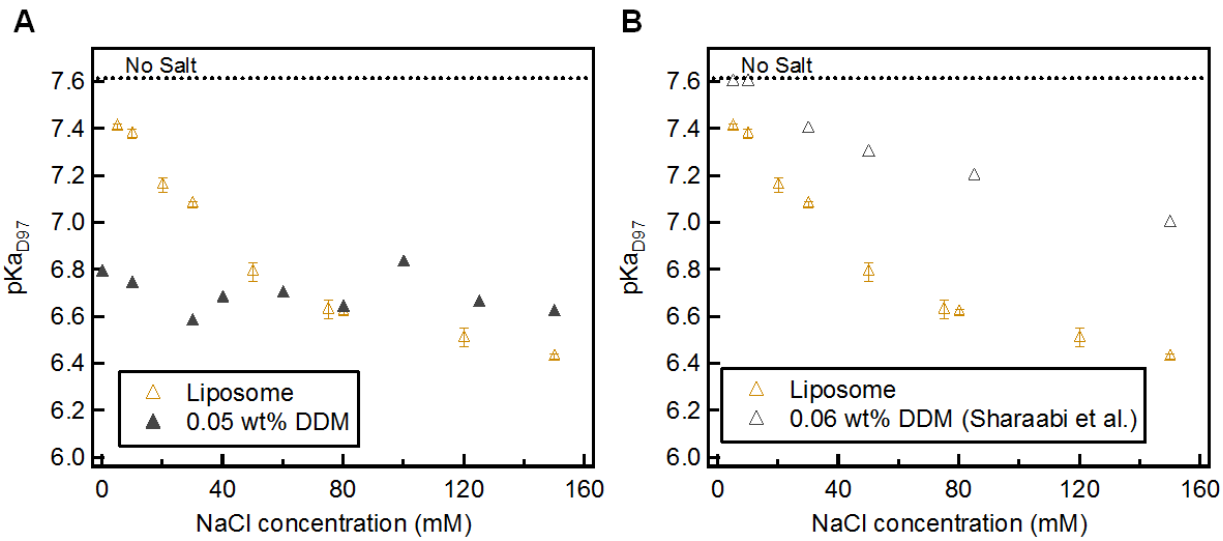

FIGURE S8 Apparent pKa_{D97} of WT PR reconstituted in POPC/POPG (80/20, mol/mol) liposomes in a HEPES buffer with various NaCl concentrations (yellow, the same set of data as in Fig. 2 A). The pKa_{D97} are compared to A. the ones of WT PR reconstituted in 0.05 wt% DDM in the same HEPES buffer with different NaCl concentrations (gray, triangle) and B. the ones of WT PR reconstituted in 0.06 wt% DDM in a Tris buffer that contains different concentrations of NaCl (gray, hollow triangle) published by Sharaabi et al (16).

Effect of hydration environment in PR-contained liposomes on apparent pKa_{D97}

Several modulators that adjust only the extent of hydration of the PR-containing liposomes were applied, one at a time, to investigate their effects on the apparent pKa_{D97}. First, the PR-contained liposome bilayer was dehydrated by adding either propranolol, a pharmaceutical drug blocker to rigidify lipid headgroup region (17), or ethanol, which reduces transient water pore formation across lipid bilayers (18). The addition of 1 mM propanolol to a HEPES buffer with 150 mM NaCl was found to have a negligible impact on the apparent pKa_{D97}, with a drop from 6.43 ± 0.02 to 6.36 ± 0.07 (Table S2). A similarly negligible pKa shift can be observed upon adding 5 wt% ethanol to the HEPES buffer containing 150 mM NaCl (pKa_{D97} = 6.75 ± 0.12). The extent of hydration of PR-containing liposomes was increased by substituting 30 mol% of the POPC with an oxidized lipid POVPC to test its effect on the apparent pKa_{D97}. The oxidized lipid POVPC with reoriented sn-2 hydrocarbon chain facilitates water penetration into the lipid bilayer to increase its hydration(19, 20). Again, no statistically significant difference was observed on the measured pKa_{D97} (6.36 ± 0.08 v.s. 6.43 ± 0.02). Overall, the applied modulators that are known to change the extent of hydration of PR-containing liposomes did not induce a significant pKa shift compared to the effect of salt concentration of the buffer. These observations suggest that the dehydration of lipid bilayers may not exert dominant effects on the pKa of embedded D97 inside PR, or that the experimental conditions and measurements are not sensitive to the relevant changes.

TABLE S2 Apparent pKa_{D97} of PR reconstituted in POPC/POPG (80/20, mol/mol) liposomes in a HEPES buffer with 150 mM of NaCl under different hydration environments adjusted by different modulators.

Condition	Effect on liposome's hydration	Apparent pKa_{D97}
Control[a]		6.43 ± 0.02
1 mM propanolol added in the buffer	Decrease(17)	6.36 ± 0.07
5 wt% EtOH added in the buffer	Decrease(18)	6.75 ± 0.12
30 mol% POVPC added in the liposome[b]	Increase(19, 20)	6.36 ± 0.08

[a] The control sample used the HEPES-NaCl buffer as described in Materials and Methods, and POPC/POPG (80/20, mol/mol) was used for the liposome composition.

[b] 30 mol% of POVPC were applied to substitute the POPG to make POPC/POVPC/POPG (50/30/20, mol/mol/mol) liposomes.

SUPPORTING REFERENCES

1. Petrache, H. I., S. Tristram-Nagle, and J. F. Nagle. 1998. Fluid phase structure of EPC and DMPC bilayers. Chemistry and physics of lipids 95:83-94.
2. Dreier, L. B., Y. Nagata, H. Lutz, G. Gonella, J. Hunger, E. H. Backus, and M. Bonn. 2018. Saturation of charge-induced water alignment at model membrane surfaces. Science advances 4:eaap7415.
3. Voinov, M. A., I. Rivera-Rivera, and A. I. Smirnov. 2013. Surface electrostatics of lipid bilayers by EPR of a pH-sensitive spin-labeled lipid. Biophysical Journal 104:106-116.
4. Cevc, G. 1990. Membrane electrostatics. Biochimica et Biophysica Acta (BBA)-Reviews on Biomembranes 1031:311-382.
5. Armstrong, B. D., and S. Han. 2007. A new model for Overhauser enhanced nuclear magnetic resonance using nitroxide radicals. The Journal of chemical physics 127:104508.
6. Armstrong, B. D., and S. Han. 2009. Overhauser dynamic nuclear polarization to study local water dynamics. Journal of the American Chemical Society 131:4641-4647.
7. Franck, J. M., A. Pavlova, J. A. Scott, and S. Han. 2013. Quantitative cw Overhauser effect dynamic nuclear polarization for the analysis of local water dynamics. Progress in nuclear magnetic resonance spectroscopy 74:33-56.
8. Hussain, S., J. M. Franck, and S. Han. 2013. Transmembrane Protein Activation Refined by Site-Specific Hydration Dynamics. Angewandte Chemie International Edition 52:1953-1958.
9. Cheng, C.-Y., J. Varkey, M. R. Ambroso, R. Langen, and S. Han. 2013. Hydration dynamics as an intrinsic ruler for refining protein structure at lipid membrane interfaces. Proceedings of the National Academy of Sciences 110:16838-16843.
10. Pavlova, A., C.-Y. Cheng, M. Kinnebrew, J. Lew, F. W. Dahlquist, and S. Han. 2016. Protein structural and surface water rearrangement constitute major events in the earliest aggregation stages of tau. Proceedings of the National Academy of Sciences 113:E127-E136.
11. Barnes, R., S. Sun, Y. Fichou, F. W. Dahlquist, M. Heyden, and S. Han. 2017. Spatially Heterogeneous Surface Water Diffusivity around Structured Protein Surfaces at Equilibrium. Journal of the American Chemical Society 139:17890-17901.
12. Nielsen, R. D., K. Che, M. H. Gelb, and B. H. Robinson. 2005. A ruler for determining the position of proteins in membranes. Journal of the American Chemical Society 127:6430-6442.
13. Holt, A., and J. A. Killian. 2010. Orientation and dynamics of transmembrane peptides: the power of simple models. European Biophysics Journal 39:609-621.
14. Segawa, T. F., M. Doppelbauer, L. Garbuio, A. Doll, Y. O. Polyhach, and G. Jeschke. 2016. Water accessibility in a membrane-inserting peptide comparing Overhauser DNP and pulse EPR methods. The Journal of chemical physics 144:194201.
15. Lueders, P., H. Jäger, M. A. Hemminga, G. Jeschke, and M. Yulikov. 2012. Multiple Pathway Relaxation Enhancement in the System Composed of Three Paramagnetic Species: Nitroxide Radical–Ln3+–O2. The journal of physical chemistry letters 3:1336-1340.
16. Sharaabi, Y., V. Brumfeld, and M. Sheves. 2010. Binding of Anions to Proteorhodopsin Affects the Asp97 pKa. Biochemistry 49:4457-4465.
17. Först, G., L. Cwiklik, P. Jurkiewicz, R. Schubert, and M. Hof. 2014. Interactions of beta-blockers with model lipid membranes: molecular view of the interaction of acebutolol, oxprenolol, and propranolol with phosphatidylcholine vesicles by time-dependent fluorescence shift and molecular dynamics simulations. European Journal of Pharmaceutics and Biopharmaceutics 87:559-569.

18. Jansen, M., and A. Blume. 1995. A comparative study of diffusive and osmotic water permeation across bilayers composed of phospholipids with different head groups and fatty acyl chains. Biophysical Journal 68:997-1008.
19. Beranova, L., L. Cwiklik, P. Jurkiewicz, M. Hof, and P. Jungwirth. 2010. Oxidation changes physical properties of phospholipid bilayers: fluorescence spectroscopy and molecular simulations. Langmuir 26:6140-6144.
20. Lis, M., A. Wizert, M. Przybylo, M. Langner, J. Swiatek, P. Jungwirth, and L. Cwiklik. 2011. The effect of lipid oxidation on the water permeability of phospholipids bilayers. Physical Chemistry Chemical Physics 13:17555-17563.